

Performance and Techno-Economic Comparison Between Solid-Particle and Molten Salt Concentrated Solar Power Systems

Ignacio Arias^{1,*} , Felipe G. Battisti² , José Cardemil¹ , Armando Castillejo-Cuberos¹ ,
and Rodrigo Escobar¹ 

¹Departamento de Ingeniería Mecánica y Metalúrgica, Escuela de Ingeniería Pontificia Universidad Católica de Chile, Chile

²Departamento de Ingeniería Mecánica, Facultad de Ingeniería, Universidad Tecnológica Metropolitana, Chile

*Correspondence: Ignacio Arias, ivarias@uc.cl

Abstract. This work presents a comprehensive comparative analysis of second-generation (Gen2) and third-generation (Gen3) concentrated solar power (CSP) technologies. The study focuses on their techno-economic performance across three diverse geographical locations: Carrera Pinto, Patache, and Santiago, in Chile. The assessment involves detailed modelling of key subsystems, including the central receiver and power block, considering daily variations and the effects of weather conditions. The results reveal that Gen2 CSP technology can achieve competitive levelized cost of energy (LCOE) values when incorporating projected cost reductions. Notably, Gen3 CSP, using solid particles as the heat transfer medium, exhibits substantial advantages due to its operation at higher temperatures (800 °C). The study also underscores the influence of local climatic conditions on CSP performance. The findings suggest that improved cost projections can render previously less attractive sites, such as Patache and Santiago, viable options for CSP deployment, underscoring the evolving landscape of renewable energy technologies.

Keywords: Concentrated Solar Power Systems, Solar Energy, Second-Generation, Third-Generation, Solid-Particles, Molten Salt

1. Introduction

The Gen3 CSP technologies have enabled significant scientific and technological advancements since the launch of the Sunshot program objectives [1]. Indeed, in the last decade, several pathways for Gen3 technology development, such as liquid, gaseous, and solid-particle pathways, have demonstrated significant advantages over Gen2 CSP technologies [2]. These advantages encompass improvements in terms of overall system efficiency, working temperatures that can exceed 800 °C, compatibility with modularization and integration with novel thermal energy storage (TES) systems, such as

packed-bed systems, latent heat storage, and thermochemical energy storage. However, certain knowledge gaps still need to be addressed [2], [3], [4]. In particular, the solid-particles pathway has proven to be a thriving field of scientific development, offering particularly attractive advantages for the CSP industry [5]. This includes the use of a chemically inert heat transfer medium in the central receiver, which remains non-reactive when in contact with the environment, experiences minimal degradation, and maintains chemical stability at temperatures exceeding 1000 °C [6], [7]. Additionally, its utilization is compatible with the concept of sensible heat particle-based TES system or indirect integration with sensible, latent, and thermochemical energy storage.

Recently, González-Portillo et al. [5] and Gunawan et al. [8] have demonstrated that solid-particle CSP systems enable achieving a LCOE around 60 \$/MWh in Dagget, California, United States. This finding is of great interest to countries pursuing an aggressive decarbonization of their electric grids as it enables the integration of renewable energies that provide firm power and a high capacity factor (CF) at a particularly low cost compared to hydropower and nuclear energy. Chile has experienced a progressive increase in installed capacity of variable renewable energies and a gradual reduction in its base load capacity through fossil fuel sources. In fact, the share of renewable energies in the total installed capacity has risen from 14% to 36.1%, while conventional sources have decreased from 82% to 63.2% from 2016 to early 2023 [9]. Therefore, technologies with high potential to achieve low LCOE and a CF are of interest for the sustainable development of Chile's electricity grid.

Due to the above, there are still unanswered questions that need to be addressed. Among these, prominent inquiries include: How does a Gen2 CSP plant compare to a Gen3 CSP plant in terms of techno-economic and performance aspects? With the anticipated cost reductions, will Gen2 CSP plants be competitive against Gen3 CSP plants?. These questions carry significant implications, particularly due to the current proximity to commercial readiness of solid-particle Gen3 CSP pathway. Indeed, in 2021, the DOE Gen3 CSP funding program selected the solid-particle heat-transfer pathway for the construction of a multi-megawatt pilot expected to commence operations in 2024. Owing to its potential to achieve a LCOE around 50 USD/MWh by 2030 and its operation significantly simpler than other development pathways. This stage places the solid particle heat transfer pathway at a technology readiness level (TRL) of TRL7 (integrated pilot system demonstration). In which is expected to mitigate key technological risks identified in the Gen3 roadmap, such as the cost of particle heat exchangers, material erosion, minimizing heat loss, and the wear and transport of particles. According to M. Imran Khan et al. [10], it is expected that Gen3 CSP systems may achieve a TRL9 (System totally proven in operational environment) by 2030, setting the stage for commercial scaling from this point onwards.

Thereby, this work aims to study and compare the performance of CSP systems based on molten salts concerning solid-particles systems, quantifying their impact on techno-economic indicators. To achieve this, a characterization of the performance for each technology was conducted, exploring the influence of different types of days on the key subsystems' performance within each scheme, such as the central receiver and power block. This detailed examination aimed to comprehend the annual techno-economic indicators, including LCOE and CF. To facilitate this understanding, the study compares three distinct sites, thereby capturing the impact of diverse local climatic conditions and radiation levels on the performance of each studied scheme.

2. Methodology

2.1 Locations under study

Both systems were analysed under different solar irradiation conditions in the extreme north, central-northern, and central regions of Chile. Specifically, the analysis included locations such as Carrera Pinto, Patache, and Santiago de Chile. The meteorological data for these locations was obtained from typical meteorological year (TMY) datasets, which were sourced from Solcast [11]. These locations were selected because they represent the typical climatological characteristics of the Atacama Desert, such as high radiation and extremely arid conditions (Carrera Pinto), high radiation with high variability (Patache), as well as the central region of Chile with a Mediterranean climate, characterized by dry summers and mild, humid winters (Santiago). The Table 1 summarizes the geographical information and radiation indices of the locations under study.

Table 1. Main geographic characteristics of the locations under study

Location	Latitude (°)	Longitude (°)	Altitude (m.a.s.l)	DNI Yearly total	GHI Yearly total (kWh/m ² -yr)	DHI Yearly total
Patache	-20.79	-70.09	610	2415.38	2277.05	632.3
Carrera Pinto	-26.96	-69.85	1920	3493.63	2500.44	324.31
Santiago	-33.49	-70.61	573	2526.2	1973.87	424.9

2.2 System descriptions and modeling considerations

For the performance assessment of solid-particle and molten salt CSP systems, computational simulations were implemented using the SolarTherm (ST) library, available for the dynamic simulation software Openmodelica [12]. Central tower technology was considered for both schemes. Simulations were performed for a TMY with meteorological and irradiation data with hourly resolution. Different combinations of TES system, solar multiple (SM), and net power (P_{net}) were analysed for both schemes. Specifically, TES configurations between 4 to 20 h with steps of 1 h, SM between 1.5 to 3.5 with steps of 0.5 and P_{net} between 50 to 100 MWe with steps of 25 MWe were assessed. The design point for both schemes correspond to the summer solstice at the solar noon with 950 W/m² of DNI with an optical efficiency of 80%. In order to have a broad analysis, the concentration factor (C) was considered that varied from 300 to 1200 for an aperture area of 1087 m² in the molten salt systems, which was considered a base case assumption of this parameter considering the by-default value considering in System Advisor Model software, while C was fixed at 2000 for solid-particle receiver due to the characteristics of direct particle heating within a cavity receiver.

Particularly, each simulation considers the computation of the optical efficiency via interpolation from an optical efficiency lookup table (OELT), which is obtained through the "Solstice.py" wrapper by mapping sun positions on a rectangular domain [13]. The OELT is interpolated through a bivariate Akima interpolation of a two-dimensional table, which uses the declination and hour angle as input elements. The molten salt CSP system follows a typical commercial configuration, i.e. uses a common mixture of 60% NaNO₃ and 40% KNO₃ as heat transfer fluid and the solar power plant is composed by a surrounding field, a cylindrical molten salt receiver, a direct TES system with two tanks for molten salts, and a power block based on a Rankine cycle with reheating, which includes an air cooled-condenser pressure. This model was constructed using SolarTherm models, such as "Sun", "ReceiverSimple_2", "HeliostatsField", "Tank",

“PumpSimple”, and “PowerBlockModel” classes. Thermochemical properties of the molten salts were obtained using the Media package, specifically the “MoltenSalt_ph” and “MoltenSalt_utilities” packages.

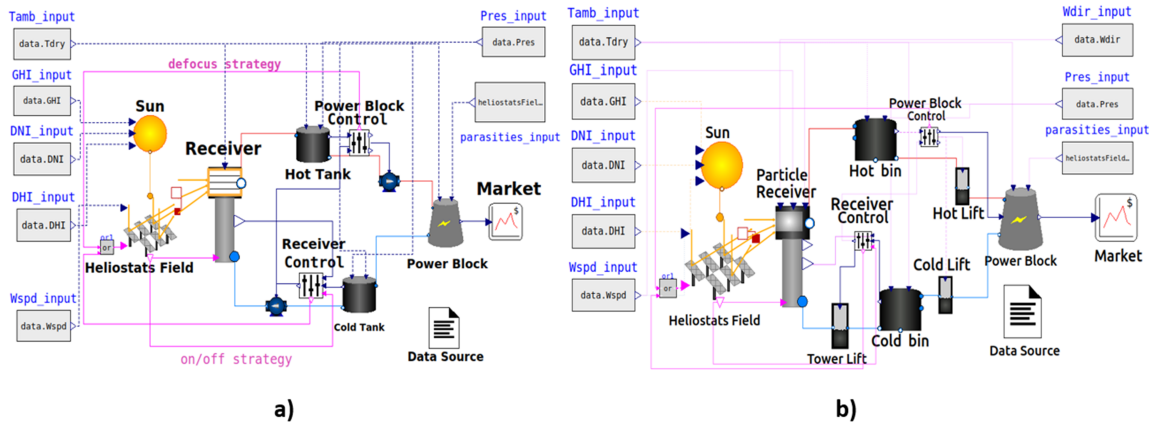


Figure 1. The system-level schemes within SolarTherm for comparison of molten salt (a) and solid-particle (b) CSP systems

The solid-particle CSP physics model uses CARBO HSP 40/70 as heat transfer medium. The solar power plant is composed by a polar heliostat field, one aperture free-falling particle receiver, a thermal energy storage system based on two ground-level particle bins, particle lifts, and a supercritical carbon dioxide (s-CO₂) Brayton cycle with recompression. This model also utilizes some class models common to the molten salt CSP model, such as “Sun” and “HeliostatsField”, nevertheless, the Gen3 CSP solid-particle based system differs significantly from a commercial CSP scheme. Therefore, it was necessary to program and integrate particle receiver, lifts, and thermal energy storage (TES) models into Openmodelica. Thereby, a comprehensive literature review was undertaken to carefully curate and select physical solid-particle subsystem models, aiming to establish a robust framework for solid-particle CSP analysis. As a result, the solid-particle CSP model is based on the works of González-Portillo et al. [14] and Gunawan et al. [8]. Specifically, the particle receiver model corresponds to a 1-D model of free-falling solid-particles with one aperture, with a view factor of 0.54 and an aspect ratio of 1. This model considers heat advection, heat conduction, and radiosity of the particle curtain and the receiver back-wall. Moreover, the particle transport system through lifts considers parasitic particle transport consumption which depends on the displacement of the lifting, the solid-particle mass flow rate and the lift efficiency (0.83), and the TES system considers energy and mass balance, as well as structural design calculations to determine the volume of refractory and concrete material to achieve a global thermal loss coefficient of approximately 2 W/K and thus significantly reduce the thermal losses. These details are comprehensively discussed in Refs. [5], [9], [13].

The power block of the molten salt CSP plant consist in a Rankine cycle with a net efficiency at the design point of 42%, while the inlet pressure at design point and the minimum turbine load were set at 100 bar and 30% of the gross power, respectively. The nominal steam mass flow rate of the power block and nominal HTF mass flow rate vary depending on the scale of the solar power plant and the hot and cold HTF temperatures were set at 565°C and 290°C, respectively. On the other hand, the power block of the solid-particle CSP plant consist in a s-CO₂ Brayton cycle with recompression with a nominal efficiency at the design point of 51%; in which, the inlet pressure at design point and the minimum turbine load were set at 250 bar and 25% of the gross

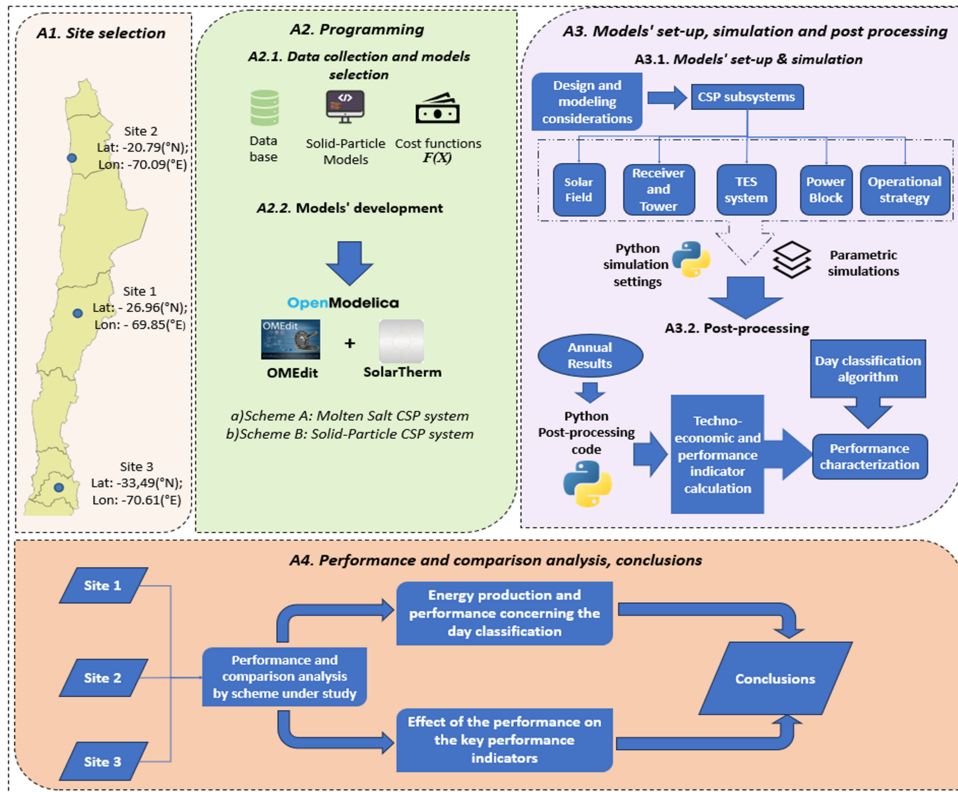


Figure 2. Methodology diagram

power, respectively. The nominal s-CO₂ mass flow rate of the power block and nominal HTF mass flow rate also vary depending on the scale of the solar power plant; however, the hot and cold bin temperatures were set at 800 °C and 550 °C, respectively. Nevertheless, the cold bin temperature will depend on the outlet temperature of the primary heat exchanger.

Each CSP model employs advanced control algorithms that effectively manage the mass flow dis-patch to the power block and receiver, utilizing the integrated “PowerBlock-Control” and “ReceiverControl” models within SolarTherm [12], [15], [16]. These sophisticated algorithms are specifically designed to dynamically adapt to various operational states, which depend on the charge status of the hot and cold bins, ensuring optimal system performance. The control strategies implemented in the CSP models are capable of precise regulation of the mass flow, allowing for the achievement of the desired temperature objective at the receiver’s outlet. The receiver control scheme carefully considers three Proportional-Integral (PI) controller states, which control the flow rate from the cold storage. By leveraging this PI control mechanism, the models can accurately adjust the flow of particles from the cold bin to maintain the target temperature at the receiver’s outlet. The precise temperature regulation plays a crucial role in maintaining the optimal operation of the CSP system, especially during varying solar radiation conditions, resulting in enhanced system performance and optimized energy output. The utilization of three PI controller states for the flow rate from the cold storage ensures precise temperature regulation at the receiver’s outlet, contributing to the overall stability and reliability of the CSP models under different operating conditions.

In the context of the power block, the control algorithms facilitate four distinct states: off, standby, partial load, and full load. This versatility in operational states allows for seamless management of the power block’s mass flow, effectively optimizing its performance based on the system’s energy demands. These control methodologies, dis-

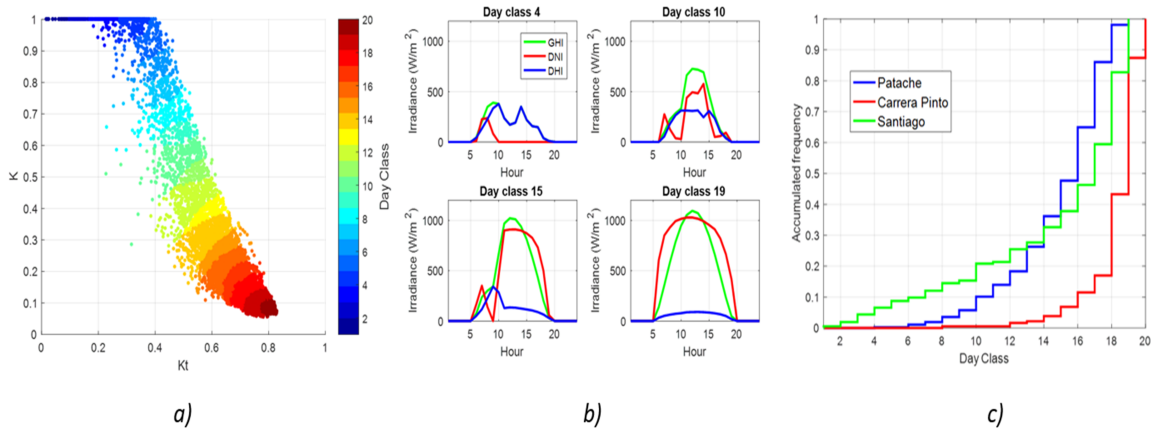


Figure 3. (a) Clearness index vs diffuse fraction concerning the day classification for the sites under study, (b) irradiance patterns for selected days and cumulative day type distributions for each location (c).

cussed in detail by Armando Fontalvo et al. [16], represent a significant advancement in the field of CSP technology, facilitating the successful integration of renewable energy sources into the grid. Additionally, the operation and dispatch strategy employed corresponds to a full energy production without dispatch restrictions and curtailment effect. Therefore, partial operation of the plant is determined by intrinsic variability and solar radiation, TES state of charge, power block response, and internal control scheme, rather than external factors.

3. Daily performance classification

To further understand how the system performs under different environmental conditions, selected performance metrics are analyzed for different types of daily irradiance patterns. To classify these patterns, the day type classification proposed by Castillejo-Cuberos and Escobar [17] was employed. However, since in this work hourly data is used, it is not possible to calculate hourly variability from sub-hourly irradiance. Therefore, a fuzzy inference system was employed to classify irradiance patterns as a function of only the clearness index and diffuse fraction that jointly, exhibited greater degrees of membership to a particular pattern classification. Gaussian membership functions were defined for each category through the mean and standard deviation for the corresponding category as determined in [17] and a maximum value defuzzifier was used to obtain the proper irradiance pattern (Day Class) value. Figure 3a depicts the different loci a particular day class pattern occupies in the clearness index Vs diffuse fraction plot to describe how different sky conditions are represented in this diagram while Figure 3b showcases the irradiance patterns for selected days. To further characterize the irradiance characteristics of these locations. Figure 3c presents the histogram of day types for each location.

Therefore, the characterization of daily performance for Gen2 and Gen3 CSP plant technologies was conducted by correlating the classification of day types with respect to two critical components of both studied plant systems: namely, the central receiver and the power block. To achieve this, utilizing the annual simulation, the daily average receiver efficiency (η_{rcv}) was determined by considering the hours of the day with an elevation angle greater than 10° . Additionally, the daily utilization factor (DUF) of the power block was defined as follows:

$$DUF = \frac{EPD[\frac{MWh}{day}]}{P_{net} \cdot 24[\frac{h}{day}]} \quad (1)$$

Where, EPD and P_{net} correspond to the energy produced by the power block per day in MWh and P_{net} is the power block nameplate capacity in MWe. Additionally, a daily characterization by day type was conducted for the thermal losses of each receiver technology with the aim of establishing and comprehending the daily efficiency outcomes. For this purpose, the daily average percentage of thermal losses with respect to the incident radiation on the aperture area ($\bar{\Phi}_{losses}$) of both receiver technologies was calculated, along with the ratio between $\bar{\Phi}_{losses}$ normalized by the receiver's aperture area (A_{rcv}). This representation portrays the capacity to transfer heat to the environment per square meter for each studied technology. Thus, $\bar{\Phi}_{losses}$ was calculated as follows:

$$\bar{\Phi}_{losses} = \frac{\dot{Q}_{rcv,loss}}{\dot{Q}_{inc}} \quad (2)$$

Where, $\dot{Q}_{rcv,loss}$ and \dot{Q}_{inc} represent the losses due to heat transfer and the incident radiation flux on A_{rcv} , respectively.

4. Techno-economic performance indicators

The annual analysis involved the evaluation of two critical indicators: the LCOE as a techno-economic metric and the CF as performance indicator. The evaluation process followed the established guidelines provided by the U.S. Department of Energy (DOE) [18]. The analysis considered key parameters such as a real discount rate of 4.4%, an annual inflation rate of 2.5%, a 30-year plant lifetime, and a construction period of 0 years. To estimate the LCOE for the CSP solid particle plant, the study utilized the cost structure proposed by Gunawan et al. [8]. Additionally, the study incorporated the cost functions reported by González-Portillo et al [5]. On the other hand, for the molten salt CSP systems, the cost functions were derived from the latest version of the System Advisor Model (SAM) [19]. Meanwhile, the cost structure was based on Refs. [20], [21], which was verified against the latest version of the NREL ATB [22]. The calculation of the LCOE was based on the established definition provided in [21] as base case. At the techno-economic level, the evaluation of both systems does not consider state subsidies. Nevertheless, notable cost differences arise due to the inherent nature of each technology, particularly in terms of Contingency, Engineering Procurement and Construction (EPC), Balance of Plant cost per gross rated power, Variable O&M cost per energy production by year, and other cost components. Notably, for the molten salt CSP system, in addition to the cost structure of the base case, cost reductions concerning the heliostat field, site preparation, and land cost per solar field aperture area were considered. This inclusion aimed to visualize the expected cost reductions in these components and their impact on the LCOE of the Gen2 CSP system. Thereby, the following equations were utilized to present the LCOE and CF:

$$LCOE = \frac{CAPEX_h + \sum_{i=n_{op}}^t \frac{OPEX_{h,i}}{(1+r)^i}}{\sum_{i=n_{op}}^t \frac{EPY_i}{(1+r)^i}} \quad (3)$$

$$CF = \frac{EPY \left[\frac{MWh}{yr} \right]}{P_{net} \cdot 8760 \left[\frac{h}{yr} \right]} \quad (4)$$

Where EPY represents the annual energy production in MWh for each respective system. On the other hand, h, r, t and n_{op} refer to the kind of CSP system - i.e. salt (ms) or particles (pcl)-, the discount rate, plant lifetime, and the year of the CSP plant's operation start, respectively. Meanwhile, CAPEX and OPEX correspond to the capital expenditures and operational expenses incurred during the analysis horizon considered in this study. The CAPEX for both molten salt and solid particle CSP schemes follow the following structure, respectively:

$$CAPEX_{ms} = C_{field} + C_{site,imp} + C_{tower} + C_{salt} + C_{rcv} + C_{tes} + C_{pb} + C_{BoP} + C_{cont} + C_{land} + C_{EPC} \quad (5)$$

$$CAPEX_{pcl} = C_{field} + C_{site,imp} + C_{tower} + C_{pcl} + C_{pcl,loss} + C_{rcv} + C_{lifts} + C_{bins} + C_{pb} + C_{BoP} + C_{cont} + C_{land} + C_{EPC} \quad (6)$$

The economic parameters for both schemes used in this study are listed in Table A1 – A3 (see appendices).

5. Results and discussion

5.1 Daily performance analysis

The locality of Carrera Pinto (Site 1), along with Gen2 CSP technology utilizing a central tower and molten salts as the Heat Transfer Fluid (HTF), was chosen as the baseline scenario to compare the performance and techno-economic indicators of different scales of this technology. This comparison was extended to include Gen3 CSP technology with central tower configuration using Solid Particles as the HTM in the receiver. The comparison was further expanded to two locations of climatic and radiative interest: Patache (Site 2) and Santiago de Chile (Site 3). These sites were selected due to their representative conditions, including the coastal effect of the Atacama Desert and the Mediterranean climate of central Chile. Two key subsystems, the central receiver, and the power block, were considered to classify and characterize the performance of both studied plant systems based on day-type classification. Figure 4 illustrates the correlation between the average daily performance of the molten salt central receiver (Figure 4a) and the solid particles receiver (Figure 4b), considering instances of the day with elevation angles greater than 10° with respect to the power block's DUF, and the day-type classification at the three studied sites.

The characterization of the receiver performance for both technologies by day-type reveals that Site 1 is suitable due to its clear sky conditions. However, contrasting the receiver performance results highlights that for days with C15 to C20 classifications—days characterized by DNI ramps due to the intrinsic variability of the solar resource and climatic conditions—along with clear days, the molten salt receiver model would enable higher average daily efficiency. This is attributed to several factors: the molten salt receiver model is a zero-dimensional model, which tends to overestimate efficiency; it accounts for greater thermal inertia due to the inclusion of the steel mass in the receiver's heat transfer; and its daily thermal losses are a fraction of the losses

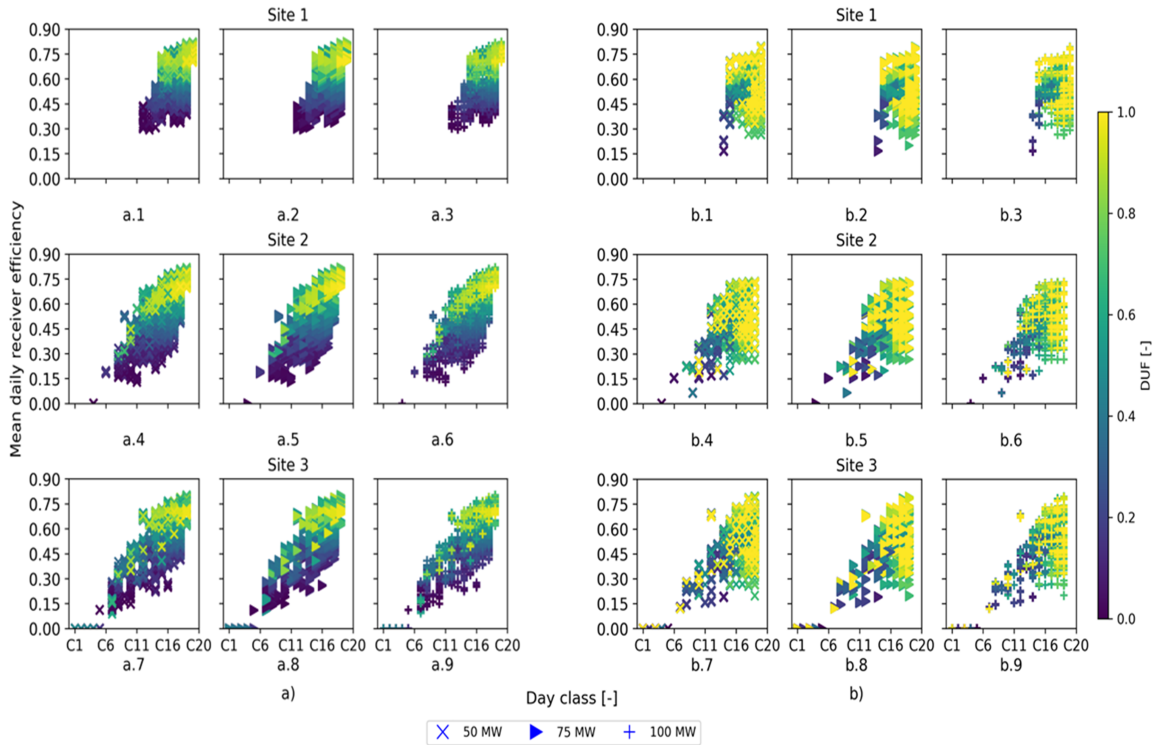


Figure 4. Correlation between the Average daily performance of the molten salt central receiver (a) and the solid-particle receiver (b) considering instances with elevation angles greater than 10° concerning the power block's DUF and the day-type classification at the three studied sites. Each row of subfigures (a) and (b) represents a site under study, while each column represents a CSP system of nameplate capacity of 50 MWe, 75 MWe, and 100 MWe, respectively.

observed in the free-falling solid particles receiver. The latter experiences heat loss due to advection, radiative losses from the particle curtain, back-wall receiver convection losses, and back-wall receiver radiosity gains, making it a more detailed model in terms of heat transfer effects.

The abovementioned observations are evident in Figure 5, which depicts the relationship between the daily average percentage of thermal losses with respect to the incident radiation on the aperture area of both receiver technologies, the classification of day types, and the ratio between the daily average percentage of thermal losses normalized by the receiver's aperture area. These relationships are illustrated across the three studied sites for different plant sizes: 50 MWe-SM=1.5- $TES=18h$, 75 MWe-SM=2.5- $TES=18h$, and 100 MWe-SM=3.5- $TES=18h$. Particularly, Figures 5a and 5b elucidate the scalability effect of the molten salt and solid particles receivers concerning thermal losses. Upon contrasting these figures, it is apparent that the molten salt receiver enables a lower daily percentage of thermal losses per square meter of receiver aperture area than the particle receiver. This disparity arises from the intrinsic characteristics of the central receiver technologies, including their geometry, the geometric relationship between the solar field and the receiver, and the receiver's susceptibility to heat transfer effects.

Considering these aspects, as previously mentioned, the design of the solar field and receiver for the molten salt and solid particles plant considers concentration factors of 600 and 2000, respectively, along with a surrounding and polar solar field configuration. The net effect of this geometric relationship, combined with the maximum allowable efficiency of both power block and receiver technologies, establishes the maximum heat flux to be concentrated on the receiver. This heat flux can be up to 31% higher

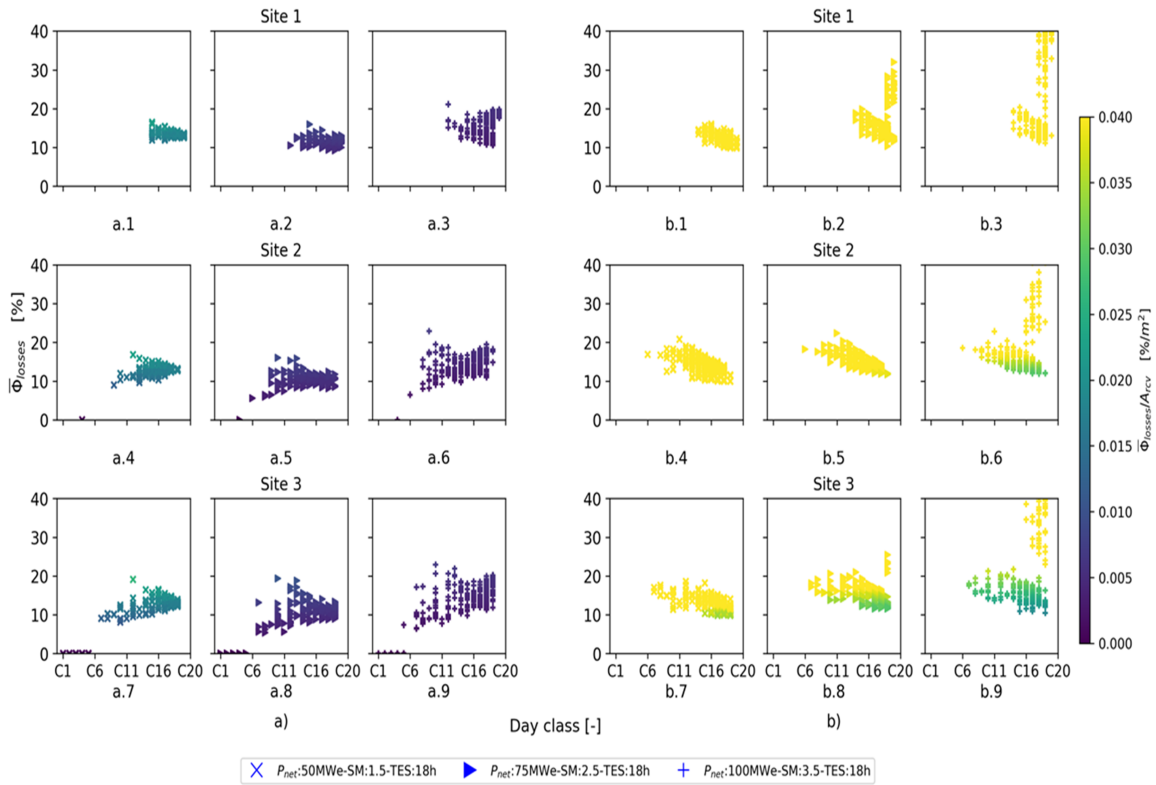


Figure 5. Illustration of $\bar{\Phi}_{losses}$ concerning the day class and the ratio between the daily average percentage of thermal losses normalized by the receiver's aperture area for Relationship between the daily average percentage of thermal losses with respect to the incident radiation on the aperture area of molten salt (a) and solid-particle (b) receivers with C of 600 and 2000, respectively.

in the molten salt receiver for a plant size of 100 MWe and SM=3.5. Moreover, this effect, combined with a larger aperture area due to a lower concentration factor, results in a lower rate of thermal losses per square meter of receiver aperture area (less than 0.015 %/m²), as depicted in Figure 5a. Meanwhile, when observing Figure 5b, the trend of the daily average percentage of thermal losses with respect to the incident radiation on the aperture area results in a more homogeneous behavior for different classifications of days encountered at the three studied sites. This behavior is due, as previously mentioned, to the intrinsic conditions of the receiver technology.

Notably, the view factor (0.54) of the free-falling particle receiver limits the radiation heat losses to the particle curtain's exposure to the air by 66%. However, this receiver technology is highly susceptible to the heat advection phenomenon due to the direct contact of the particle curtain with the air, and therefore it exhibits an intrinsic sensitivity to the size of the CSP plant, specifically to the height of the central tower, as well as the wind speed and direction profile. This latter aspect is evident in Figure 5b, where for the three studied sites, at 100 MWe and a solar multiple of 3.5, corresponding to a tower height of over 250 m, on clear days with classifications between 17 and 20, and high wind speeds (over 15 m/s), daily average losses of around 25% are recorded. Although the thermal losses represent between 10% to 20% of the incident radiation on the receiver, the increase in the concentration factor and a lower maximum heat flux to be concentrated on the receiver translate to a smaller aperture area for the receiver. Consequently, the ratio between the daily average percentage of thermal losses normalized by the receiver's aperture area can be 7 times higher than the values obtained using the molten salt receiver model.

6. Annual techno-economic performance

Concerning the techno-economic analysis, Figure 6 illustrates the correlation among the LCOE, TES hours, and CF for several diverse configurations of Gen2 CSP plants which are contemplated in the present study. This analysis considers the cost structure for the years 2023 (depicted in Figure 6a) and 2030 (depicted in Figure 6b) respectively. Where, each row of subfigures (a) and (b) represents a site under study, while each column represents a CSP system of nameplate capacity of 50 MWe, 75MWe, and 100 MWe, respectively. As is evident from Figure 6a, the cost structure corresponding to the year 2023 allows for LCOE values around 73 \$/MWh for a Gen2 CSP plant of 100 MWe with a SM of 2.5 and a TES capacity of 14 hours in Carrera Pinto. In contrast, for the evaluations conducted in Patache and Santiago de Chile, all plant configurations surpass LCOE values of 91 \$/MWh. As is widely acknowledged in the literature, locations with DNI exceeding 2000 kWh/m²-yr are considered ideal for the deployment of CSP plants, such as Patache and Santiago de Chile. However, locations characterized by a higher frequency of overcast days and/or greater variability in solar radiation throughout the day affect the operation of critical components within the CSP plant, as illustrated in Figure 3c. This diminishes energy production and impacts indicators like LCOE and CF, regardless of the installed capacity.

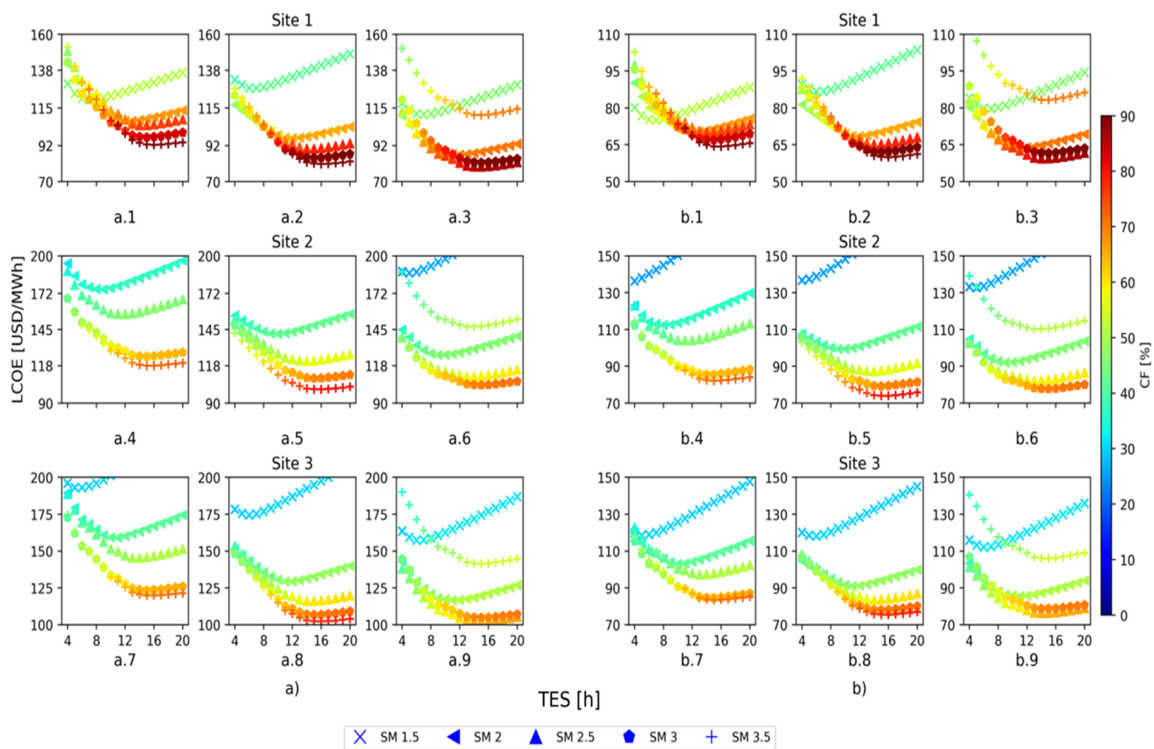


Figure 6. LCOE vs. hours of storage and SM concerning the CF for molten salt with cost structure for (a) 2023 and (b) 2030 for an aperture area of 1087 m²

Nevertheless, by considering a cost structure for Gen2 CSP that integrates the projected cost reductions for Gen3 heliostats, as well as the anticipated cost reductions by 2030 for the TES system, power block, central tower, and receiver for Gen2 CSP plants (refer to Figure 6-b), it can be observed that the LCOE value drops to a minimum of approximately 59 \$/MWh for a 100 MWe Gen2 CSP plant with an SM of 3 and a TES capacity of 14 hours in Carrera Pinto. Meanwhile, in locations such as Patache and Santiago de Chile, this cost structure allows achieving LCOE values as low as 72 \$/MWh and CF values exceeding 90%. These results provide insight into how CSP cost

projections could enable the re-evaluation of sites like Patache or Santiago de Chile, which are currently considered unattractive in terms of techno-economic factors. This re-evaluation would involve assessing their relevance and feasibility when presented as alternatives to other renewable energy sources for electricity generation.

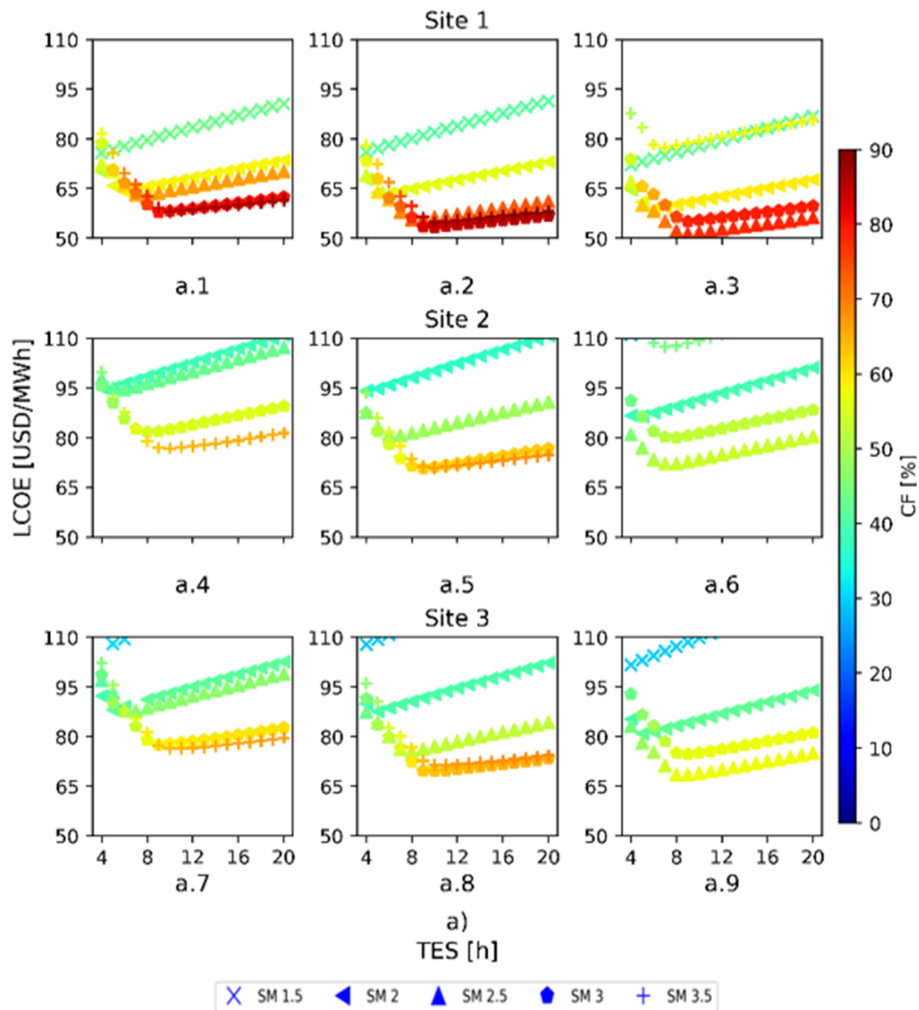


Figure 7. LCOE vs. TES capacity and SM concerning the CF for solid-particle CSP system. Results for a $C=2000$ in all the simulation routines

Regarding the techno-economic evaluation of the Gen3 CSP scheme, Figure 7 compiles the results of the assessment for nominal power, SM, and TES capacity across the three studied sites. Where, each row of subfigures (a) represent a site under study, while each column represents a CSP system of nameplate capacity of 50 MWe, 75 MWe, and 100 MWe, respectively. These outcomes reveal that despite the fact that the particle receiver is more sensitive to thermal losses and, consequently, exhibits a higher thermal losses ratio per square meter in absolute terms, operating at high temperatures, employing a design with a concentration factor of 2000, and benefiting from the inherent cost reduction due to the construction simplicity of the particle receiver as well as the TES system, enables achieving LCOE values of approximately 52 \$/MWh. This represents approximately 11.8% lower than the minimum LCOE result obtained for CSP Gen2 technology at Carrera Pinto, considering the cost structure projected for 2030 considering the cost structure projected for 2030, and an 28.82% lower than the corresponding 2023 cost structure. Additionally, it is observed that CSP Gen3 technology based on solid particles will allow reaching minimum LCOE values

for Patache and Santiago, between 70–75 \$/MWh for 8-12 hours of TES, and a solar multiple ranging from 2.5 to 3.5, regardless of the installed capacity.

7. Conclusions

This work conducted a comprehensive comparison between Gen2 and Gen3 CSP technologies, focusing on central tower configurations with molten salt and solid particles as heat transfer fluids. The site selection, including Carrera Pinto, Patache, and Santiago de Chile, considered the local solar radiation conditions. Carrera Pinto, characterized by clear skies, emerged as an optimal location for both technologies. However, the inherent variability in solar radiation in Patache and Santiago resulted in performance variations, impacting key indicators like LCOE and CF. In fact, locations with high DNI, such as Patache and Santiago, can seem favorable, but their frequent cloud cover and variable solar radiation can lead to operational challenges and reduced energy production. These effects negatively influence key performance metrics, such as LCOE and CF, underlining the need for careful site selection and accurate resource assessment.

On the other hand, the study underscored the potential benefits of incorporating the projected cost reductions of Gen3 technologies into the cost structure of Gen2 CSP systems. Taking into account the anticipated cost decline in heliostats and TES systems, the LCOE of the Gen2 CSP plant in Carrera Pinto was significantly reduced, reaching values of approximately 59 \$/MWh. This highlights the value of harnessing technological advancements and economies of scale to enhance the cost competitiveness of CSP systems. It demonstrates that Gen2 technology will continue to be viable and compete with the new generations of CSP technologies. Despite the above, this aforementioned, this work considers a system-level comparison involving single-aperture free-falling particle receivers, which limits the capture of solar radiation from the surrounding solar field. Therefore, it is proposed to complement these results by incorporating an analysis of multi-aperture particle receivers. The research demonstrated the importance of detailed receiver models in capturing the nuances of performance. While simpler models may overestimate efficiency, they might underestimate factors like heat losses. The detailed analysis using advanced models provides a more accurate representation of thermal losses and, consequently, a better assessment of plant performance. As a result, future work should focus on conducting a more comprehensive comparison by employing a highly detailed model of the molten salt receiver. This approach would ensure a level playing field in terms of modeling complexity and enhance the validity of the comparative analysis.

Author contributions

Ignacio Arias: Conceptualization, Methodology, Software, Validation, Formal analysis, Investigation, Resources, Data curation, Writing – original draft, Writing – review & editing, Visualization, Supervision. Felipe G. Battisti: Investigation, Writing – review & editing, Visualization, Supervision. José Cardemil: Investigation, Writing – review & editing, Supervision. Armando Castillejo-Cuberos: Investigation, Writing – review & editing, Supervision. Rodrigo Escobar: Investigation, Writing – review & editing, Supervision, Resources, Writing – original draft.

Competing interests

The authors declare that they have no known competing financial interests or personal relationships that could have appeared to influence the work reported in this paper.

Funding

Ignacio Arias acknowledges the funding from ANID PFCHA/Doctorado Nacional 2021-21210053. Felipe G. Battisti acknowledges the funding from ANID/FONDECYT Project 3220792. Armando Castillejo-Cuberos acknowledges the funding from ANID/ FONDECYT Project 3220686.

Acknowledgement

Ignacio Arias would like to thank L. F. González-Portillo for the feedback on the CSP model based on solid-particles.

Appendix

Table A.1. Cost structure assumed for solid-particle CSP subsystems [5], [8]

Parameter	Value	Unit
Risk and EPC Process Details		
Contingency (of CAPEX)	10	%
Engineering procurement and construction (EPC) (of CAPEX)	9	%
Operation cost		
Fixed O&M cost per nameplate power by year	40	\$/W
Variable O&M cost per energy production by year	3	\$/MWh
Balance of Plant cost per gross rated power	0.167	\$/kWe
Solar field and central receiver-tower system		
Field cost per solar field aperture area	75	\$/m ²
Site preparation cost per solar field aperture area	10	\$/m ²
Land cost	2.471	\$/m ²
Solid-Particle receiver cost per receiver aperture area	37400	\$/m ²
Tower cost	depends on the cost function	\$
Lifts specific cost	58.37	\$/m ³ (kg/s)
Thermal storage system		
Refractory material	2700	\$/m ³
High density concrete	850	\$/m ³
Portland concrete	229	\$/m ³
Floor filler material	150	\$/m ³
Solid-Particle CARBO HSP 40/70	1	\$/kg
Primary Heat Exchanger		
Heat exchanger cost per heat transfer area	6594.5	\$/m ²
Particle horizontal feeder	9153	\$/kg/s
sCO ₂ piping cost	4753	\$/kg/s
Power Block		
Power block cost	depends on the cost functions	\$/kWe

Table A.2. Cost structure assumed for 2023 by subsystems for molten salt CSP system [19], [21]

Parameter	Base case	Unit
Risk and EPC Process Details		
Contingency (of CAPEX)	7	%
Engineering procurement and construction (EPC) (of CAPEX)	11	%
Operation cost		
Fixed O&M cost per nameplate power by year	56.715	\$/W
Variable O&M cost per energy production by year	3.5	\$/MWh
Balance of Plant cost per gross rated power	290	\$/kWe
Solar field and central receiver-tower system		
Heliostat Field cost per solar field aperture area	127	\$/m ²
Site preparation cost per solar field aperture area	16	\$/m ²
Land cost	2.471	\$/ m ²
Receiver cost per receiver aperture area	103,000,000	USD
Receiver reference area	1,571	m ²
Receiver cost scaling exponent	0.7	-
Tower cost	3,000,000	USD
Tower cost scaling exponent	0.0113	
Thermal storage and power block		
Power block	1000	\$/kWe
Thermal storage	22	\$/kWh _{th}

Table A.3. Cost structure assumed for 2030 by subsystems for molten salt CSP system [20]

Parameter	Expected scenario	Unit
Risk and EPC Process Details		
Contingency (of CAPEX)	5	%
Engineering procurement and construction (EPC) (of CAPEX)	9	%
Operation cost		
Fixed O&M cost per nameplate power by year	45	\$/W
Variable O&M cost per energy production by year	3.5	\$/MWh
Balance of Plant cost per gross rated power	200	\$/kWe
Solar field and central receiver-tower system		
Heliostat Field cost per solar field aperture area(a)	75	\$/m ²
Site preparation cost per solar field aperture area(a)	10	\$/m ²
Land cost	2.471	\$/m ²
Tower cost	72000	\$/m
Receiver cost	90	\$/kW _{th}
Thermal storage and power block		
Power block	900	\$/kWe
Thermal storage	18	\$/kWh _{th}

References

- [1] "Sunshot vision study — department of energy," Accessed: Mar. 31, 2024. [Online]. Available: <https://www.energy.gov/eere/solar/sunshot-vision-study>.
- [2] M. Mehos et al., "Concentrating solar power gen3 demonstration roadmap," National Renewable Energy Lab. (NREL), Golden, CO (United States), Tech. Rep., Jan. 2017. DOI: [10.2172/1338899](https://doi.org/10.2172/1338899). [Online]. Available: <https://www.osti.gov/biblio/1338899>.
- [3] I. Arias, J. Cardemil, E. Zarza, L. Valenzuela, and R. Escobar, "Latest developments, assessments and research trends for next generation of concentrated solar power plants using liquid heat transfer fluids," *Renewable and Sustainable Energy Reviews*, vol. 168, p. 112 844, 2022, ISSN: 1364-0321. DOI: <https://doi.org/10.1016/j.rser.2022.112844>. [Online]. Available: <https://www.sciencedirect.com/science/article/pii/S1364032122007262>.
- [4] C. K. Ho, "A review of high-temperature particle receivers for concentrating solar power," *Applied Thermal Engineering*, vol. 109, pp. 958–969, 2016, Special Issue: Solar Energy Research Institute for India and the United States (SERIUS) – Concentrated Solar Power, ISSN: 1359-4311. DOI: <https://doi.org/10.1016/j.applthermaleng.2016.04.103>. [Online]. Available: <https://www.sciencedirect.com/science/article/pii/S1359431116305919>.
- [5] L. F. González-Portillo, K. Albrecht, and C. K. Ho, "Techno-economic optimization of csp plants with free-falling particle receivers," *Entropy*, vol. 23, no. 1, 2021, ISSN: 1099-4300. DOI: [10.3390/e23010076](https://doi.org/10.3390/e23010076). [Online]. Available: <https://www.mdpi.com/1099-4300/23/1/76>.
- [6] C. K. Ho et al., "Gen 3 particle pilot plant (g3p3) – high-temperature particle system for concentrating solar power (phases 1 and 2)," Sandia National Lab. (SNL-NM), Albuquerque, NM (United States), Tech. Rep., Nov. 2021. DOI: [10.2172/1832285](https://doi.org/10.2172/1832285). [Online]. Available: <https://www.osti.gov/biblio/1832285>.
- [7] C. K. Ho et al., "Overview and design basis for the gen 3 particle pilot plant (g3p3)," *AIP Conference Proceedings*, vol. 2303, no. 1, p. 030 020, Dec. 2020, ISSN: 0094-243X. DOI: [10.1063/5.0029216](https://doi.org/10.1063/5.0029216). eprint: https://pubs.aip.org/aip/acp/article-pdf/doi/10.1063/5.0029216/14223138/030020_1_online.pdf. [Online]. Available: <https://doi.org/10.1063/5.0029216>.
- [8] P. G. Gan, W. Ye, and P. John, "System Modelling and Optimization of a Particle-Based CSP System," *The Australian National University: Canberra, Australia*, 2021.
- [9] C. N. de Energía. "Información y estadísticas - comisión nacional de energía," Accessed: Mar. 31, 2024. [Online]. Available: <https://www.cne.cl/nuestros-servicios/reportes/informacion-y-estadisticas/>.
- [10] M. Imran Khan, F. Asfand, and S. G. Al-Ghamdi, "Progress in technology advancements for next generation concentrated solar power using solid particle receivers," *Sustainable Energy Technologies and Assessments*, vol. 54, p. 102 813, 2022, ISSN: 2213-1388. DOI: <https://doi.org/10.1016/j.seta.2022.102813>. [Online]. Available: <https://www.sciencedirect.com/science/article/pii/S221313882200861X>.
- [11] J. M. Bright, "Solcast: Validation of a satellite-derived solar irradiance dataset," *Solar Energy*, vol. 189, pp. 435–449, 2019, ISSN: 0038-092X. DOI: <https://doi.org/10.1016/j.solener.2019.07.086>. [Online]. Available: <https://www.sciencedirect.com/science/article/pii/S0038092X19307571>.

- [12] P. Scott, A. d. I. C. Alonso, J. T. Hinkley, and J. Pye, "Solartherm: A flexible modelica-based simulator for csp systems," *AIP Conference Proceedings*, vol. 1850, no. 1, p. 160 026, Jun. 2017, ISSN: 0094-243X. DOI: [10.1063/1.4984560](https://doi.org/10.1063/1.4984560). eprint: https://pubs.aip.org/aip/acp/article-pdf/doi/10.1063/1.4984560/13748442/160026\1_online.pdf. [Online]. Available: <https://doi.org/10.1063/1.4984560>.
- [13] Y. Wang et al., "Verification of optical modelling of sunshape and surface slope error for concentrating solar power systems," *Solar Energy*, vol. 195, pp. 461–474, 2020, ISSN: 0038-092X. DOI: <https://doi.org/10.1016/j.solener.2019.11.035>. [Online]. Available: <https://www.sciencedirect.com/science/article/pii/S0038092X19311338>.
- [14] L. F. González-Portillo, V. Soria-Alcaide, K. Albrecht, C. K. Ho, and B. Mills, "Benchmark and analysis of a particle receiver 1d model," *Solar Energy*, vol. 255, pp. 301–313, 2023, ISSN: 0038-092X. DOI: <https://doi.org/10.1016/j.solener.2023.03.046>. [Online]. Available: <https://www.sciencedirect.com/science/article/pii/S0038092X23002062>.
- [15] A. de la Calle, A. Bayon, and J. Pye, "Techno-economic assessment of a high-efficiency, low-cost solar-thermal power system with sodium receiver, phase-change material storage, and supercritical co2 recompression brayton cycle," *Solar Energy*, vol. 199, pp. 885–900, 2020, ISSN: 0038-092X. DOI: <https://doi.org/10.1016/j.solener.2020.01.004>. [Online]. Available: <https://www.sciencedirect.com/science/article/pii/S0038092X20300049>.
- [16] A. Fontalvo et al., "System-level comparison of sodium and salt systems in support of the gen3 liquids pathway," *AIP Conference Proceedings*, vol. 2445, no. 1, p. 030 007, May 2022, ISSN: 0094-243X. DOI: [10.1063/5.0087911](https://doi.org/10.1063/5.0087911). eprint: https://pubs.aip.org/aip/acp/article-pdf/doi/10.1063/5.0087911/16203159/030007\1_online.pdf. [Online]. Available: <https://doi.org/10.1063/5.0087911>.
- [17] A. Castillejo-Cuberos and R. Escobar, "Understanding solar resource variability: An in-depth analysis, using chile as a case of study," *Renewable and Sustainable Energy Reviews*, vol. 120, p. 109 664, 2020, ISSN: 1364-0321. DOI: <https://doi.org/10.1016/j.rser.2019.109664>. [Online]. Available: <https://www.sciencedirect.com/science/article/pii/S136403211930869X>.
- [18] C. DOE. "Gen 3 csp topic 1–phase 3 test facility down-selection criteria: Technical report."
- [19] NREL. "Csp cost data - system advisor model - sam.," Accessed: Mar. 31, 2023. [Online]. Available: <https://sam.nrel.gov/concentrating-solar-power/csp-cost-data.html>.
- [20] A. Zurita, C. Mata-Torres, J. M. Cardemil, and R. A. Escobar, "Evaluating different operation modes of a hybrid csp+pv+tes+bess plant varying the dispatch priority," *AIP Conference Proceedings*, vol. 2126, no. 1, p. 090 007, Jul. 2019, ISSN: 0094-243X. DOI: [10.1063/1.5117609](https://doi.org/10.1063/1.5117609). eprint: https://pubs.aip.org/aip/acp/article-pdf/doi/10.1063/1.5117609/14190260/090007\1_online.pdf. [Online]. Available: <https://doi.org/10.1063/1.5117609>.
- [21] A. Zurita, C. Mata-Torres, J. M. Cardemil, R. Guédez, and R. A. Escobar, "Multi-objective optimal design of solar power plants with storage systems according to dispatch strategy," *Energy*, vol. 237, p. 121 627, 2021, ISSN: 0360-5442. DOI: <https://doi.org/10.1016/j.energy.2021.121627>. [Online]. Available: <https://www.sciencedirect.com/science/article/pii/S0360544221018752>.
- [22] *Data — electricity — 2023 — atb — nrel*. [Online]. Available: <https://atb.nrel.gov/electricity/2023/data>.